Research Article Vol. 31, No. 18 / 28 Aug 2023 / Optics Express 29166
Optics EXPRESS

# On-chip generation of adjustable cylindrical vector beams

C. Cisowski,[1,*] C. Klitis,[2] P. Maidment,[2] M. Sorel,[2] and S. Franke-Arnold[1]

[1]School of Physics and Astronomy, University of Glasgow, G12 8QQ, Glasgow, Scotland, UK
[2]James Watt School of Engineering, University of Glasgow, G12 8QQ, Glasgow, Scotland, UK
*clairemarie.cisowski@glasgow.ac.uk

**Abstract:** Cylindrical vector (CV) beams have sparked considerable interest due to their extraordinary vectorial properties, desirable for applications ranging from microscopy to high energy physics. Increasing demand for cost-effective, small-footprint photonics has fueled the development of photonic integrated circuits (PICs) capable of generating structured light beams in recent years. This technology however suffers from low reconfigurability, limiting the variety of CV beams that can be generated from these devices. In this article, we propose a novel design to overcome this limitation, which exploits the polarization-dependent response of annular gratings embedded into a microring resonator to generate re-configurable CV beams. We demonstrate the viability of the device in a proof-of-principle experiment including spatially resolved Stokes measurements.



## 1. Introduction

The Silicon-on-Insulator (SOI) platform supports the realization of telecommunication technologies [1], biosensors [2,3], spectrometers [4,5], imaging systems [6] and logic circuits [6,7]. Its greatest strength lies in its compatibility with metal oxide semiconductor technology, resulting in low-cost, high-volume assembly capacities [8]. The development of integrated light sources has been the focus of considerable research efforts [9,10] as it holds transformative potential for strategic areas including medical imaging and wearable sensors. The integration of structured light sources with spatially dependent phase and/or polarization distributions, has become a priority in virtue of their superior information-carrying capacities [11], their ability to control trapped particles [12,13] and their applications in quantum optics [14–16].

In 2012, X. Cai et al. introduced an integrated optical vortex emitter based on a silicon microring resonator [17]. The device relied on an annular grating, engraved into the inner side of the microring, to couple the confined whispering gallery modes (WGMs) into free space and to impose an azimuthal phase variation to the emitted beam. Variations of this design, including the combination of several concentric ring resonators [18], superimposed gratings [19], a slant configuration [20], and families of unidirectional resonators [21] to cite a few, have been proposed subsequently. Interestingly, the beam of light generated by the resonator also presents a space-variant polarization profile, characteristic of a cylindrical vector (CV) beam [17]. CV beams, including radially polarized and azimuthally polarized light beams, possess intriguing focusing properties [22] and have found applications in nanoscale optical imaging [23]. It was demonstrated experimentally that quasi-transverse electric polarized WGMs emit light beams that are predominantly azimuthally polarized [17], while radially polarized CV beams can be obtained by changing the polarization of the WGMs and by modifying the angular phase matching conditions [18]. A grating embedded on top of the microring resonator can generate both radially polarized and azimuthally polarized CV beams upon switching the polarization and

#494462 https://doi.org/10.1364/OE.494462
Journal © 2023 Received 28 Apr 2023; revised 21 Jul 2023; accepted 9 Aug 2023; published 16 Aug 2023

Optics EXPRESS

wavelength of the access waveguide driving the resonator [24]. Both Ref. [17] and Ref. [24] used a polarizer to test their theoretical predictions experimentally, however these measurements are not sufficient to fully characterize the polarization distribution of the field.

We present a novel design that exploits the the polarization dependence of WGMs confined in a silicon microring resonator to built a versatile integrated CV generator, capable of generating a continuous range of CV modes on demand. Our device presents two inner gratings, one optimized for transverse electric (TE) WGMs and one optimized for transverse magnetic (TM) WGMs. We show numerically that the gratings produce orthogonal CV modes and demonstrate how their combined response can generate a large variety of CV modes simply by tuning the phase and amplitude of the mode in the access waveguide. We confirm our predictions experimentally by taking spatially resolved Stokes measurements on the generated CV beams from our prototype device and discuss next steps to improve its performance. This work lays the foundations for a novel generation of integrated multi-CV beam emitters, with implications for medical imaging, particle manipulation and communications.

## 2. Proposed design

Introducing a grating on the inner sidewalls of a microring resonator enables coupling the confined WGMs into radiative cylindrical modes in the vertical direction $z$, i.e. perpendicular to the plane $(x, y)$ of the integrated circuit (see Fig. 1(a)). Free space emission is conditioned by the angular phase-matching relation [17]:

$$\nu_{\mathrm{rad}} = p - gq, \tag{1}$$

where $g = \pm 1, \pm 2, \ldots$ is the diffraction order, $p$ is the azimuthal order of the WGMs, which corresponds to the number of optical periods around the resonator and $q$ is the number of grating elements. $\nu_{\mathrm{rad}}$ measures the azimuthal phase shift of the radiated beam and defines the topological charge, $\ell$, quantizing the amount of orbital angular momentum carried by the beam.

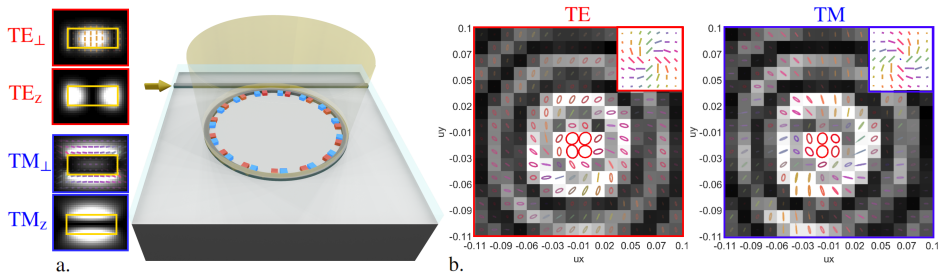


**Fig. 1.** (a) Schematic of the proposed device geometry, showing the normalized intensity and polarization distributions of the quasi-TE and quasi-TM modes on a silicon waveguide with cross section 500×220 nm (left). Two gratings, optimized for TE and TM input, respectively, are represented in different colors. (b) Simulated far-field intensity distribution of the vertically emitted beams obtained from TE and TM input, respectively, showing the polarization distributions as overlay. The corresponding ideal CV modes $\psi_1, \psi_2$ are shown as insets. The ellipses are color coded to distinguish between different polarization states.

The polarization distribution of the radiated beam is determined by the local polarization state of the confined optical field at each grating element [25]. The symmetry of the annular grating indicates that the radiated beam should present a cylindrical polarization pattern. We consider a ring resonator and an access waveguide fabricated on standard silicon waveguides of cross section 500×220 nm, embedded between silica lower and upper cladding. These waveguides support quasi-TE modes and quasi-TM modes, with polarization profiles and normalized intensity

Optics EXPRESS

distributions as shown in Fig. 1(a). Here $TE_\perp$, $TM_\perp$ are calculated from the components of the electric field in the cross section of the waveguide and $TE_\parallel$, $TM_\parallel$ are deduced from the component of the electric field along the waveguide.$TE_\perp$ is confined to the centre of the waveguide and possesses a strong $TE_\parallel$ component primarily located on the sidewalls [26] whereas the quasi-TM mode stretches in the vertical direction (see Fig. 1(a)).

Annular gratings located on the top of the waveguide strongly interact with $TE_\perp$ and $TM_\parallel$ modes, leading to the emission of radially and azimuthally polarized modes, respectively, as evidenced in [24]. Precise control over the depth of the grating is required for engineering the strength of the top grating. This can be technologically challenging, hence a sidewall grating can sometimes be preferable. Sidewall gratings interact more strongly with quasi-TE modes than quasi-TM modes and, as discussed in [24], both $TE_\perp$ and $TE_\parallel$ contribute to the overall polarization response, making it difficult to obtain pure azimuthal or radial polarization responses. Nevertheless sidewall gratings are capable of generating azimuthally polarized CV beams based on experimental polarization measurements involving a single polarizer [17].

The focus of our preliminary investigations is the simulation of the polarization distribution of the mode emitted by a ring resonator with gratings defined on the inner sidewall. We consider a ring resonator of 20 µm radius, which offers a good compromise between compact footprint and negligible bending losses. A 100 nm gap. associated with a coupling coefficient of 0.16, separates the ring resonator from the access waveguide. The lower and upper cladding consist of a 2 µm-thick and a 1 µm-thick silicon dioxide layer, respectively. To facilitate subsequent investigations, we assume that the resonator emits light carrying topological charge $\ell = 0$ at a wavelength $\lambda_0 = 1550$nm under TE and TM excitation, respectively. We also assume that the amplitudes of the so-obtained radiated modes are equal. Because the effective refractive indices of the quasi-TE and quasi-TM modes differ significantly, with $n_{\text{eff}}(\text{TE}) = 2.44$ and $n_{\text{eff}}(\text{TM}) = 1.77$ in a straight $500 \times 220\,\text{nm}^2$ silicon waveguide at $\lambda_0$, we design two gratings, optimized separately for TE and TM input (indicated in red and blue in Fig. 1(a)). This difference in effective refractive indices ensures independent response to TE and TM responses, vertical emission only occurring when the Bragg condition is met [27]. We used a grating period of 637 nm for TE input (197 elements) and of 897 nm for TM input (140 elements). TE grating elements are $60 \times 60\,\text{nm}^2$ squares, whereas TM grating elements have a width of 60 nm and protrudes from the inner ring by a depth of 80nm, allowing us to increase the strength of the radiated mode for TM input to match the amplitude of the TE radiated mode.

Fig. 1(b) shows the simulated far field intensity and polarization distribution of the radiated beams generated by the TE-optimized grating and the TM-optimized grating, respectively. The intensity profiles are obtained using 3D finite-difference time-domain simulations using the software Ansys-Lumerical. The far field is calculated on a hemispherical surface at a distance of one meter from the ring resonator. The spatial grid is constructed from unitary directional vectors where $-1 \leq u_{x,y} \leq +1$. The polarization distributions of the obtained radiated modes in the first diffraction order correspond to the desired ideal CV modes, $\psi_1, \psi_2$ shown as insets in Fig. 1(b). In the basis of circularly polarized Laguerre-Gaussian ($\text{LG}_\text{p}^\ell$) modes, $\psi_1$ and $\psi_2$ are usually defined as:

$$\begin{aligned} \psi_1 &= i\,\text{LG}_0^1\sigma_- + \text{LG}_0^{-1}\sigma_+, \\ \psi_2 &= -i\,\text{LG}_0^1\sigma_- + \text{LG}_0^{-1}\sigma_+, \end{aligned} \tag{2}$$

where $\sigma_\mp$ denotes right-and left-handed circularly polarized light, respectively. Much like a pair of radially polarized and azimuthally polarized modes, $\psi_1$ and $\psi_2$ occupy diametrically opposite positions on the higher-order Poincaré sphere of CV modes shown in Fig. 2 [28]. Consequently, one can generate various CV modes $\Psi$ as a superposition of the basis modes $\psi_1$ and $\psi_2$:

$$\Psi = a\exp(i\varphi)\psi_1 + b\psi_2 \tag{3}$$

Optics EXPRESS

where $a$ and $b$ are relative mode weightings and $\varphi$ is a relative phase difference. Fig. 2(a) illustrates how a continuous range of CV modes can be obtained by tuning the relative phase difference of $\psi_1$ and $\psi_2$ at equal weighting, whereas Fig. 2(b) shows CV modes obtained by varying the relative mode weights for $\varphi = 0$ (lower arc) and $\varphi = \pi$ (upper arc). In practice, this indicates that a ring resonator presenting two sidewall gratings, one optimized for TE modes and the other for TM modes, can generate adjustable CV beams in a fixed geometry. The polarization distribution of the radiated mode is controlled by tuning the relative weight and phase of the TE and TM modes excited in the access waveguide. The technology to exert phase and amplitude control directly on silicon chips has reached a mature stage [29], providing a significant advantage to our design. We therefore have a very simple yet robust multi-CV emitter scheme.

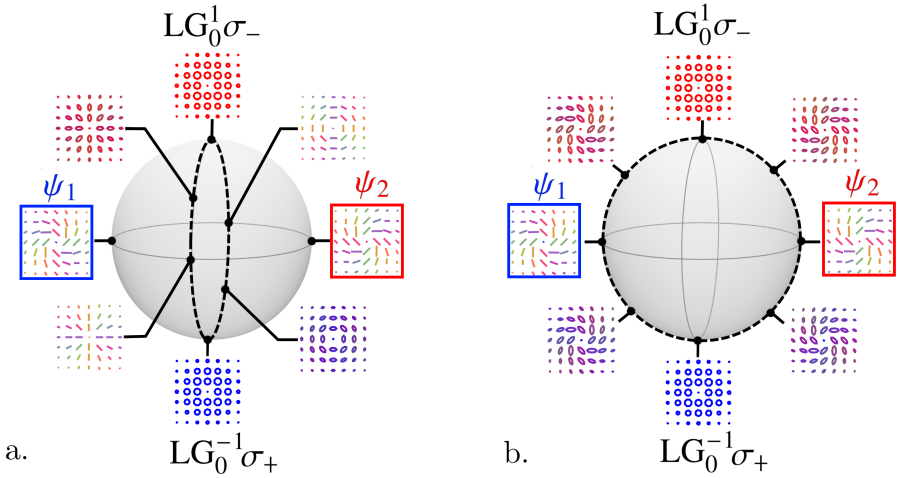


**Fig. 2.** Higher-order Poincaré sphere ($|\sigma| \neq \ell$, $\ell = 1$) of CV modes. All points on this sphere can be written as a superposition of the two basis modes, situated at the poles, chosen to be $\psi_1$ and $\psi_2$, which correspond to circularly polarized LG modes. In (a), the bold dashed circle represents the position on the sphere of all CV modes that can be obtained by varying the relative phase between $\psi_1$ and $\psi_2$ for an equally weighted sum of $\psi_1$ and $\psi_2$. In (b), the bold dashed circle indicates all CV modes obtained by varying the amplitude between $\psi_1$ and $\psi_2$ for a fixed relative phase. In both cases, the polarization distribution of some of these modes are provided for illustration.

We now proceed to demonstrate experimentally that a silicon ring presenting two annular gratings can generate the predicted $\psi_1$ and $\psi_2$ CV modes under TE and TM excitation. We also show how the two modes can be combined to create a novel CV mode as a proof of concept.

## 3. Experimental realization and discussion

The waveguide devices were defined in a negative tone resist using electron-beam lithography. The pattern was then dry-etched into the 220nm silicon using a reactive-ion etch with a mixed chemistry of $SF_6/C_4F_8$, followed by the deposition of a $1\mu$m-thick silicon dioxide passivation layer. Several microrings with slightly different grating parameters were manufactured on the same silicon chip for testing as the estimated fabrication tolerance was $\approx$ 10nm (see Table 1).

Figure 3 shows a schematic illustration of the experimental setup used to study the radiated CV modes. The light source is a tunable InGaAsP DBR Laser with a 1520-1620 nm wavelength range. A paddle-based fibre polarization controller, acting as two quarter waveplates (QWP) and a half waveplate (HWP), is used to adjust the polarization state of the incoming mode. We have chosen to control the amplitude and phase of the TE and TM modes outside of the silicon chip in

Optics EXPRESS

**Table 1. Grating parameters of the eight manufactured silicon ring resonators.**

| | | R1 | R2 | R3 | R4 | R5 | R6 | R7 | R8 |
|---|---|---|---|---|---|---|---|---|---|
| TE grating | Period (nm) | 637 | 634 | 634 | 634 | 637 | 637 | 634 | 641 |
| | Size (nm) | 60×60 | 60×80 | 60×80 | 60×80 | 60×60 | 60×60 | 60×120 | 60×80 |
| TM grating | Period (nm) | 897 | 897 | 891 | 904 | 891 | 904 | 897 | 897 |
| | Size (nm) | 60×80 | 60×80 | 60×80 | 60×80 | 60×80 | 60×80 | 60×120 | 60×80 |

this proof of principle experiment for simplicity. The fibre exciting the access waveguide is a single-mode lensed fibre of spot diameter 2.5±0.5 µm, it is placed on an xyz-translation stage for alignment purposes.The CV modes emitted vertically from the sample are collected by a x10 achromatic microscope objective, a QWP followed by a polarizer are used to perform spatially resolved Stokes polarimetry. The camera used for imaging is an 320 x 256 pixels Hamamatsu c10633 InGaAs camera with a 30 µm pitch.

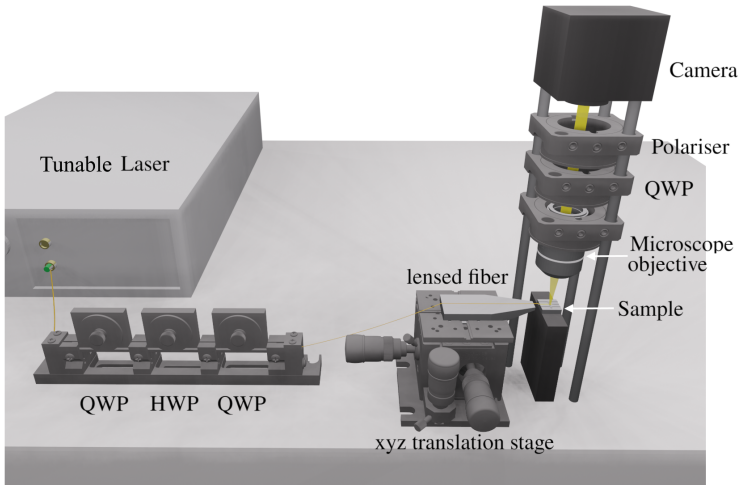


**Fig. 3.** Representation of the experimental setup used to analyze the radiated CV modes.

The CV modes corresponding to TE and TM inputs are shown in Fig. 4(a,b). These correspond to our best measurements of $\psi_1$ and $\psi_2$, they were obtained from R1 at $\lambda = 1551$nm and from R2 at $\lambda = 1543$nm, respectively. These results were reproducible across many rings, producing distinct $\psi_1$ and $\psi_2$ mode responses when either TE or TM modes were excited. Fig. 4(c) shows a specific example of CV beam obtained for an intermediary polarization state exciting R2 at $\lambda = 1543$nm, obtained from an equally weighted superposition of $\psi_1$ and $\psi_2$ with $\varphi = 0$ in Eq. (3). As predicted by Fig. 2, we have thus confirmed experimentally that annular circular gratings emit the predicted fundamental $\psi_1, \psi_2$ CV modes and that these modes can be combined to generate other CV modes.

We have identified several areas of improvement for future designs. Firstly, we found that obtaining a 50/50 ratio of $\psi_1$ and $\psi_2$ at $\lambda_0$ was a challenging task as these were usually emitted at slightly different frequencies. This facilitated our measurements of the individual responses of the TE and TM gratings; however, this made the measurement of the combined response challenging. Fine tuning of the combined resonance conditions will require further manufacturing optimizations and testing slightly different grating periods. Secondly, it appears that while using a tunable laser source is advantageous to correct discrepancies between simulated and real resonance frequencies one important drawback for our experiment was the polarization

Optics EXPRESS

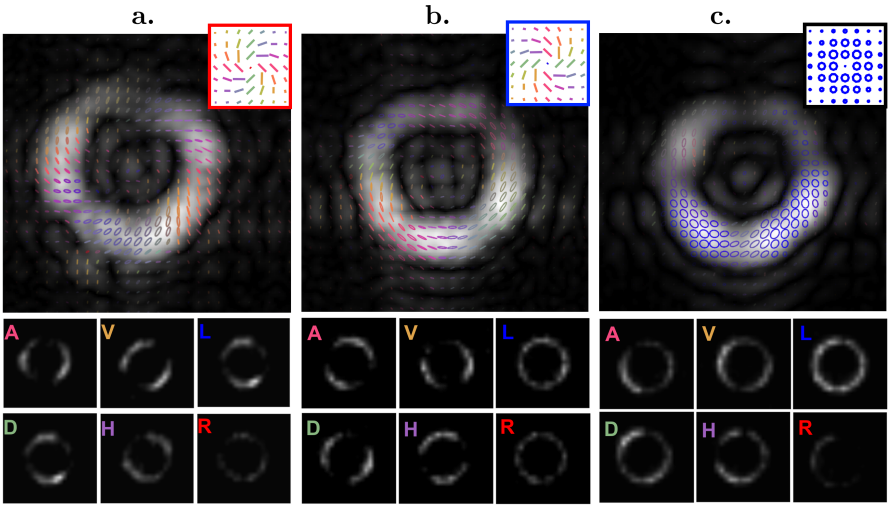


**Fig. 4.** Experimental intensity distributions of the radiated CV modes, along with their polarization distribution as an overlay for (a). (b) TE input. (c) TM input. An intermediary input. The theoretical polarization distributions are shown as insets on the top right of each image. The respective experimental polarization measurements used to reconstruct the polarization distribution are provided under each image where A stands for linear anti-diagonal, D linear diagonal, V linear vertical, H linear horizontal, L left-handed circularly polarized and R right-handed circularly polarized.

instabilities associated with the laser internal Fabry-Perot cavity [30] which made precise relative phase and amplitude control of TE and TM modes almost impossible. The solution would thus be to use a different laser source once the manufacturing parameters for $\lambda_0$ operation are established.

## 4. Conclusion

In summary, we have introduced a novel adjustable CV beam generator based on a silicon ring resonator. We have shown that two sidewall gratings, positioned in the inner side of the ring, generate two CV modes that can be combined to obtain other CV modes simply by controlling the relative phase and amplitude of the TE and TM modes propagating in the access waveguide used to excite the ring. We confirmed our theoretical predictions in a proof of principle experiment. Implementing polarization control directly on the silicon chip, using variable amplitude splitters and thermo-electric phase shifters, for instance, should be considered in the future iterations of the device as this will not only allow for precise tuning but will also contribute to reducing the footprint of the device. In principle, gratings situated on the top of the silicon rings can also be combined to generate tunable CV modes using a single geometry, however whether this geometry is more advantageous from sidewall gratings remains to be determined. Our device paves the way for novel generation of compact CV beams emitters with applications for imaging, sensing and particle manipulation.

**Funding.** Royal Society (NIF/R1/192384).

**Acknowledgments.** C.M.C. acknowledges financial support from the Royal Society through an International Newton fellowship NIF/R1/192384. The authors acknowledge insightful discussions with Sebastian Schulz upon designing the ring resonator. C.M. Cisowki, M. Sorel and S. Franke-Arnold conceived the work. C.M. Cisowski built the numerical model under the guidance of C. Klitis. P. Maidment was involved in the construction of the experimental setup. C. M. Cisowski gathered and analyzed the data with M. Sorel and S. Franke-Arnold overseeing the theoretical analysis. All authors have contributed to writing the manuscript.

Optics EXPRESS

**Disclosures.** The authors declare that the research was conducted in the absence of any commercial or financial relationships that could be construed as a potential conflict of interest.

**Data availability.** The datasets generated and analyzed during the study are available from [31].

## References


1. C. R. Doerr, "Silicon photonic integration in telecommunications," Front. Phys. **3**, 37 (2015).
2. M. Iqbal, M. A. Gleeson, B. Spaugh, F. Tybor, W. G. Gunn, M. Hochberg, T. Baehr-Jones, R. C. Bailey, and L. C. Gunn, "Label-free biosensor arrays based on silicon ring resonators and high-speed optical scanning instrumentation," IEEE J. Sel. Top. Quantum Electron. **16**(3), 654–661 (2010).
3. G.-J. Zhang and Y. Ning, "Silicon nanowire biosensor and its applications in disease diagnostics: A review," Anal. Chimica Acta **749**, 1–15 (2012).
4. M. Yu, Y. Okawachi, A. G. Griffith, N. Picqué, M. Lipson, and A. L. Gaeta, "Silicon-chip-based mid-infrared dual-comb spectroscopy," Nat. Commun. **9**(1), 1869 (2018).
5. L. Tombez, E. J. Zhang, J. S. Orcutt, S. Kamlapurkar, and W. M. J. Green, "Methane absorption spectroscopy on a silicon photonic chip," Optica **4**(11), 1322–1325 (2017).
6. C. Rogers, A. Y. Piggott, D. J. Thomson, R. F. Wiser, I. E. Opris, S. A. Fortune, A. J. Compston, A. Gondarenko, F. Meng, X. Chen, G. T. Reed, and R. Nicolaescu, "A universal 3D imaging sensor on a silicon photonics platform," Nature **590**(7845), 256–261 (2021).
7. R. Santagati, J. W. Silverstone, M. J. Strain, M. Sorel, S. Miki, T. Yamashita, M. Fujiwara, M. Sasaki, H. Terai, M. G. Tanner, C. M. Natarajan, R. H. Hadfield, J. L. O'Brien, and M. G. Thompson, "Silicon photonic processor of two-qubit entangling quantum logic," J. Opt. **19**(11), 114006 (2017).
8. L. Tsybeskov, D. J. Lockwood, and M. Ichikawa, "Silicon photonics: Cmos going optical [scanning the issue]," Proc. IEEE **97**(7), 1161–1165 (2009).
9. Z. Wang, A. Abbasi, and U. Dave, *et al.*, "Novel light source integration approaches for silicon photonics," Laser Photonics Rev. **11**(4), 1700063 (2017).
10. L. Feng, Z. J. Wong, R.-M. Ma, Y. Wang, and X. Zhang, "Single-mode laser by parity-time symmetry breaking," Science **346**(6212), 972–975 (2014).
11. J. Wang, J.-Y. Yang, I. M. Fazal, N. Ahmed, Y. Yan, H. Huang, Y. Ren, Y. Yue, S. Dolinar, M. Tur, and A. E. Willner, "Terabit free-space data transmission employing orbital angular momentum multiplexing," Nat. Photonics **6**(7), 488–496 (2012).
12. L. Paterson, M. P. MacDonald, J. Arlt, W. Sibbett, P. E. Bryant, and K. Dholakia, "Controlled rotation of optically trapped microscopic particles," Science **292**(5518), 912–914 (2001).
13. M. P. MacDonald, L. Paterson, K. Volke-Sepulveda, J. Arlt, W. Sibbett, and K. Dholakia, "Creation and manipulation of three-dimensional optically trapped structures," Science **296**(5570), 1101–1103 (2002).
14. R. Fickler, R. Lapkiewicz, W. N. Plick, M. Krenn, C. Schaeff, S. Ramelow, and A. Zeilinger, "Quantum entanglement of high angular momenta," Science **338**(6107), 640–643 (2012).
15. M. Mirhosseini, O. S. Maga na-Loaiza, M. N. O'Sullivan, B. Rodenburg, M. Malik, M. P. J. Lavery, M. J. Padgett, D. J. Gauthier, and R. W. Boyd, "High-dimensional quantum cryptography with twisted light," New J. Phys. **17**(3), 033033 (2015).
16. A. Forbes and I. Nape, "Quantum mechanics with patterns of light: Progress in high dimensional and multidimensional entanglement with structured light," AVS Quantum Sci. **1**(1), 011701 (2019).
17. X. Cai, J. Wang, M. J. Strain, B. Johnson-Morris, J. Zhu, M. Sorel, J. L. O'Brien, M. G. Thompson, and S. Yu, "Integrated compact optical vortex beam emitters," Science **338**(6105), 363–366 (2012).
18. S. A. Schulz, T. Machula, E. Karimi, and R. W. Boyd, "Integrated multi vector vortex beam generator," Opt. Express **21**(13), 16130–16141 (2013).
19. Q. Xiao, C. Klitis, S. Li, Y. Chen, X. Cai, M. Sorel, and S. Yu, "Generation of photonic orbital angular momentum superposition states using vortex beam emitters with superimposed gratings," Opt. Express **24**(4), 3168–3176 (2016).
20. Y. Sebbag and U. Levy, "Arbitrarily directed emission of integrated cylindrical vector vortex beams by geometric phase engineering," Opt. Lett. **45**(24), 6779–6782 (2020).
21. W. E. Hayenga, M. Parto, J. Ren, F. O. Wu, M. P. Hokmabadi, C. Wolff, R. El-Ganainy, N. A. Mortensen, D. N. Christodoulides, and M. Khajavikhan, "Direct generation of tunable orbital angular momentum beams in microring lasers with broadband exceptional points," ACS Photonics **6**(8), 1895–1901 (2019).
22. K. S. Youngworth and T. G. Brown, "Focusing of high numerical aperture cylindrical-vector beams," Opt. Express **7**(2), 77–87 (2000).
23. Q. Zhan, "Cylindrical vector beams: from mathematical concepts to applications," Adv. Opt. Photonics **1**(1), 1–57 (2009).
24. Z. Shao, J. Zhu, Y. Zhang, Y. Chen, and S. Yu, "On-chip switchable radially and azimuthally polarized vortex beam generation," Opt. Lett. **43**(6), 1263–1266 (2018).
25. Z. Shao, J. Zhu, Y. Chen, Y. Zhang, and S. Yu, "Spin-orbit interaction of light induced by transverse spin angular momentum engineering," Nat. Commun. **9**(1), 926 (2018).
26. J. B. Driscoll, X. Liu, S. Yasseri, I. Hsieh, J. I. Dadap, and R. M. Osgood, "Large longitudinal electric fields (ez) in silicon nanowire waveguides," Opt. Express **17**(4), 2797–2804 (2009).

Optics EXPRESS

27. C. Klitis, G. Cantarella, M. J. Strain, and M. Sorel, "High-extinction-ratio te/tm selective bragg grating filters on silicon-on-insulator," Opt. Lett. **42**(15), 3040–3043 (2017).
28. G. Milione, H. I. Sztul, D. A. Nolan, and R. R. Alfano, "Higher-order Poincaré sphere, Stokes parameters, and the angular momentum of light," Phys. Rev. Lett. **107**(5), 053601 (2011).
29. G. T. Reed, G. Mashanovich, F. Y. Gardes, and D. J. Thomson, "Erratum: Silicon optical modulators," Nat. Photonics **4**(9), 660 (2010).
30. A. Ejlli, F. Della Valle, and G. Zavattini, "Polarisation dynamics of a birefringent Fabry–Perot cavity," Appl. Phys. B **124**(2), 22 (2018).
31. C. Cisowski, "On-chip generation of reconfigurable cylindrical vector beams," University of Glasgow (2023).https://doi.org/10.5525/gla.researchdata.1428